Discover Oncology

Case Report

Molecular genetic analysis of pulmonary benign metastasizing leiomyoma and intravenous leiomyomatosis: a comparative study using whole exome sequencing

Jin Li[1,2] · Jiafei Zeng[1] · Shuai Luo[1] · Jinjing Wang[1]

Received: 13 January 2025 / Accepted: 2 May 2025
Published online: 28 May 2025

Abstract

Objective Benign Metastasizing Leiomyoma (BML) and Intravenous Leiomyomatosis (IVL) are rare uterine-derived smooth muscle tumors. Although both exhibit histologically benign and similar features, they demonstrate aggressive biological behaviors. Currently, molecular genetic studies on BML and IVL are limited, and no comparative research on their genetic variations has been reported. To investigate the genetic basis underlying their shared aggressive phenotypes, this study employs whole-exome sequencing (WES) to conduct a molecular genetic comparison between the two entities. The aim is to explore potential genetic variations that may reveal common pathological pathways shared by these diseases, thereby enhancing our understanding of the molecular mechanisms driving their invasiveness.

Methods A pulmonary BML case and an IVL case underwent analysis, with paraffin-embedded tumor tissues subjected to WES. Mutant genes were screened and comparatively analyzed between the two cases.

Results WES revealed 15 single nucleotide polymorphism (SNP) genetic mutations in the BML case: HFM1, SCN10A, HEXA, SLC7A14, TEP1, KCNJ12, KCNJ18, DNAJB12, ACOX3, ABCC2, RASA1, ALOX15B, TCIRG1, COL5A3, and MCCC2. In the IVL case, 18 mutant genes were observed: CADPS2, GPSM2, REEP4, KCNJ12, KCNJ18, DUSP15, PDE11A, TCIRG1, KLHL33, PAH, MYO18A, FBLN7, ATP7B, MYO7A, MLKL, LRP10, KRT15, and HEPH. The mutations were consistent across both samples in this case. Shared mutations in BML and IVL cases included TCIRG1, KCNJ12, and KCNJ18.

Conclusion BML and IVL exhibit distinct gene mutations in tumor development, with certain shared mutations.

Keywords Benign metastasizing leiomyoma · Intravenous leiomyomatosis · Whole exome sequencing · Pathology · Mutations in genes

Abbreviations

BML	Benign metastasizing leiomyoma
IVL	Intravenous leiomyomatosis
SNP	Single nucleotide polymorphism
WES	Whole exome sequencing
CT	Computed tomography
DWI	Diffusion weighted imaging

✉ Jinjing Wang, jinjingwangls@163.com | [1]Department of Pathology, Affiliated Hospital of Zunyi Medical University, Zunyi, Guizhou, People's Republic of China. [2]Department of Pathology, Tongren People's Hospital, Tongren, Guizhou, People's Republic of China.

1 Background

BML and IVL, originating from uterine smooth muscle cells, present similar histomorphological features [1]. Although BML is histomorphologically benign, it demonstrates distant metastasis, primarily affecting the lungs [2]. In contrast, IVL proliferates within uterine veins, extending through venous blood flow to involve extrauterine vessels. Existing molecular genetic research on BML and IVL is sparse, lacking comparative mutation analyses. This study employed WES on paraffin-embedded tumor tissues from BML and IVL cases to explore their molecular genetic profiles. The analysis observed 15 pathogenic single nucleotide polymorphism (SNP) genes in BML cases and 18 pathogenic mutations in IVL cases. Notably, TCIRG1, KCNJ12, and KCNJ18 mutations were shared mutant genes in both BML and IVL cases.

2 Materials and methods

2.1 Case presentation

2.1.1 Case one

A 52-year-old postmenopausal woman, who had a hysterectomy for a uterine tumor at age 29 and was pathologically diagnosed with uterine leiomyoma, presented with left-sided chest pain of unknown cause and no other abnormal symptoms or signs on April 1, 2023. She was a non-smoker and non-drinker with no pre-existing conditions. After admission, a chest X-ray revealed multiple nodules in both lungs, suggestive of metastatic tumors. Contrast-enhanced chest computed tomography (CT) scans confirmed multiple nodules of varying sizes in both lungs, with the largest, approximately 18 mm in diameter, located in the right lower lobe with a well-defined boundary. Some nodules exhibited heterogeneous enhancement, indicating bilateral metastatic lung tumors (Fig. 1). On May 11, 2023, a thoracoscopic wedge resection of the left upper and lower lung lobes was performed. Biopsy and pathological examination revealed gray-white nodules in the left lower and upper lobes, measuring approximately $1.0 \times 0.5 \times 0.5$ cm and $1.5 \times 1.0 \times 1.0$ cm, respectively, with well-defined boundaries and a solid, gray-white, and tough nature. Histological analysis confirmed benign leiomyoma with no malignant features (Fig. 2). Immunohistochemical staining showed tumor cells expressing Vimentin, h-Caldesmon, Desmin, SMA, ER, and PR, with a Ki-67 positive rate of about 2% in the hotspot area (Fig. 3). CD10, CD34, and S-100 were negative. The bronchoalveolar epithelium within the nodule was positive for TTF1 antibody. Given the patient's history of uterine leiomyoma, the final diagnosis was BML in the left upper and lower lung lobes. Postoperatively, the patient recovered well without special treatment. A 13-month follow-up showed the disease remained well-controlled, with no metastasis detected elsewhere.

2.1.2 Case two

A 60-year-old postmenopausal woman, who had a hysterectomy and bilateral adnexectomy at age 50 for uterine tumors, was pathologically diagnosed with uterine leiomyoma post-surgery. She had no history of smoking, alcohol consumption, or pre-existing conditions. A chest CT scan conducted approximately 10 years after surgery revealed small scattered pulmonary

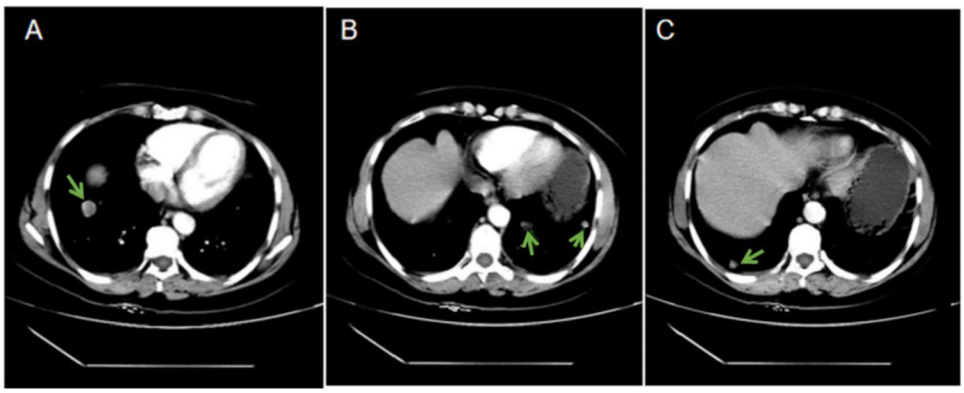

Fig. 1 **A**–**C** Contrast-enhanced chest CT scan identified multiple nodules in both lungs, some displaying heterogeneous enhancement(As indicated by the green arrow)

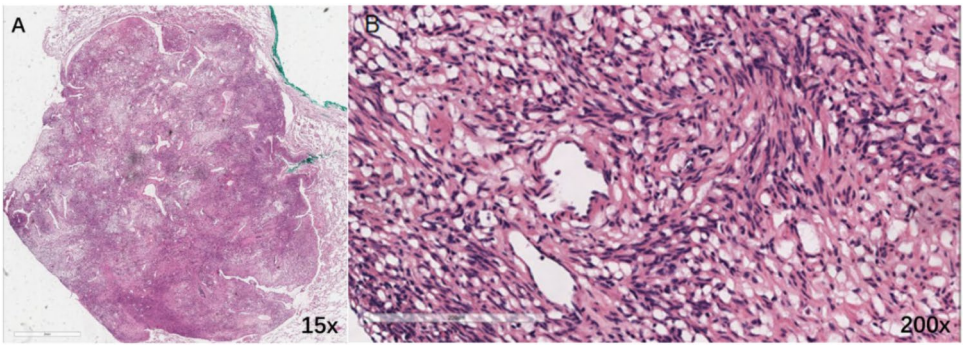

Fig. 2 Histological examination of left lung nodules revealed well-defined boundaries with surrounding tissues, comprising spindle cells of uniform size and mild morphology, arranged in a woven pattern. The cells exhibited no significant atypia, infrequent nuclear divisions, unapparent nucleoli, and an absence of necrosis. Scattered bronchial alveolar epithelial cells, morphologically normal, were present in the nodules (A Hematoxylin and eosin H&E × 15; **B** H&E × 200

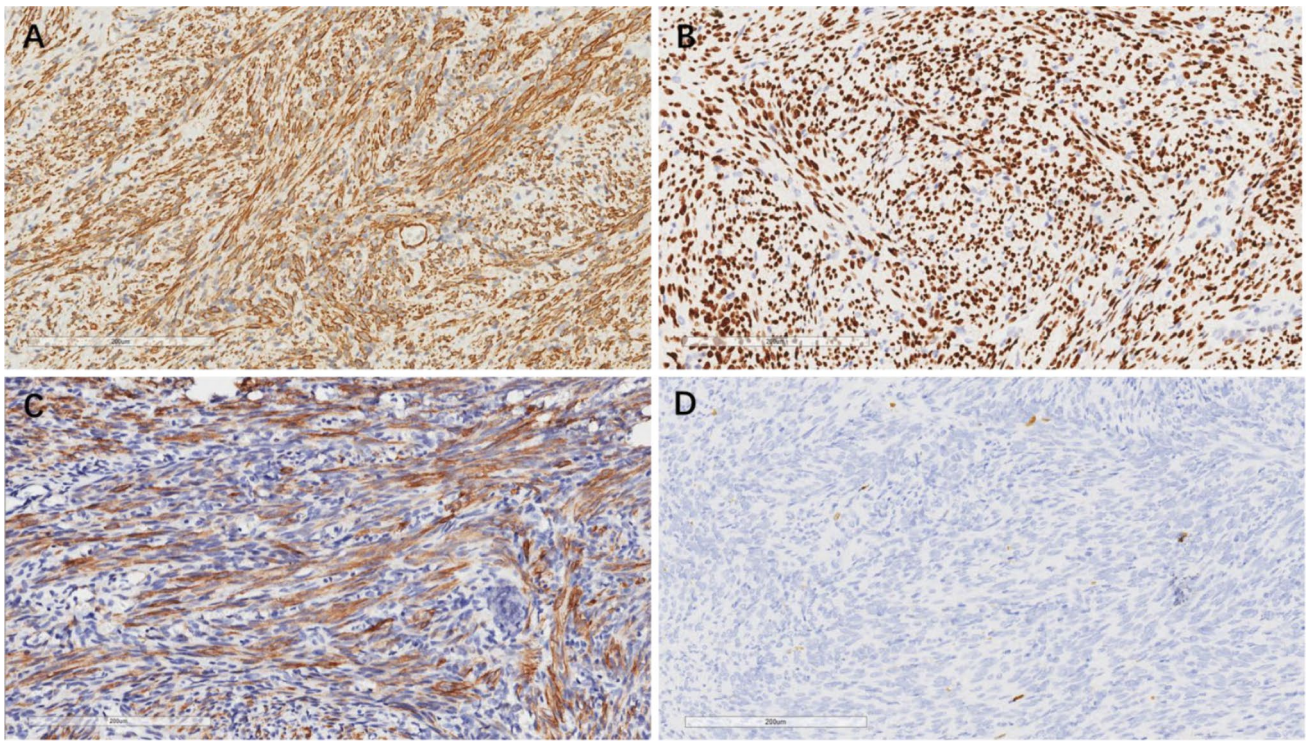

Fig. 3 **A** IHC staining revealed positive SMA expression in the cytoplasm of spindle cells, **B** ER positivity in the nuclei of spindle cells, **C** h-Caldesmon positivity in the cytoplasm of spindle cells, D: nuclear Ki-67 positivity in approximately 2% of cells. EnVision, × 200

nodules, measuring between 3 and 11 mm in diameter. Contrast-enhanced CT of the abdomen and pelvis revealed a right pelvic mass measuring approximately 81 × 58 × 10 mm (Fig. 4). The right internal iliac vein exhibited heterogeneous density, thickening, and an indistinct boundary with the pelvic tumor. Pelvic magnetic resonance imaging (MRI) confirmed the absence of the uterus, irregular soft tissue thickening at the stump, significant enhancement on contrast scans, and some nodular enhancement. A right pelvic tumor with a homogeneous signal, approximately 8.9 × 5.1 × 9.9 cm, was observed. It presented with irregularly lobular T1 equisignal and T2 slightly short signals, well-defined edges, restricted diffusion on diffusion weighted imaging (DWI), and notable homogeneous enhancement on contrast scans; it was closely associated with the vaginal stump. Imaging results, coupled with the patient's medical history, indicated the recurrence of smooth muscle tumors post-surgery (Fig. 5). The patient underwent pelvic tumor resection, during which the tumor was found in the right iliac fossa retroperitoneal area, measuring approximately 9.5 × 8.5 × 5 cm. It exhibited a tough nature, abundant blood supply, and lobulated shape, with the base attached to the left wall of the vaginal stump (Fig. 6). Intraoperative exploration revealed

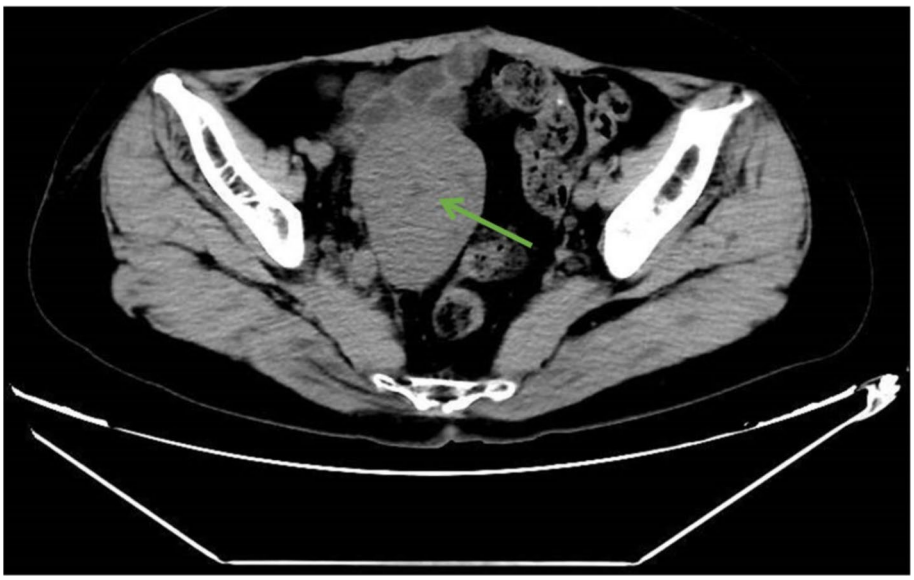

Fig. 4 The mass was in the right pelvic cavity (As indicated by the green arrow)

Fig. 5 The enhanced scan of the pelvic mass demonstrated significant enhancement, closely associated with the vaginal stump

thickening of the right internal iliac vein, which contained a stripe-like tumor measuring approximately 15 × 5 × 2 cm, with a tough nature and pale color, which was excised. Postoperatively, biopsy specimens from the left wall of the vaginal stump and the right internal iliac vein mass underwent histopathological examination. Both lesions exhibited identical histological features, characterized by the morphological hallmarks of benign smooth muscle tumors, with no malignant morphological characteristics observed (Fig. 7). Immunohistochemical staining showed positive expressions of Vimentin, SMA, Desmin, H-caldesmon, ER, and PR, with a Ki-67 positive rate of approximately 3% in the hotspot area (Fig. 8). Markers such as CD10, CD34, and CD117 were unexpressed. The final diagnosis was intravascular and vaginal stump leiomyomatosis. The patient received no additional treatment post-surgery and recovered well, with no recurrence observed after 10 months of follow-up.

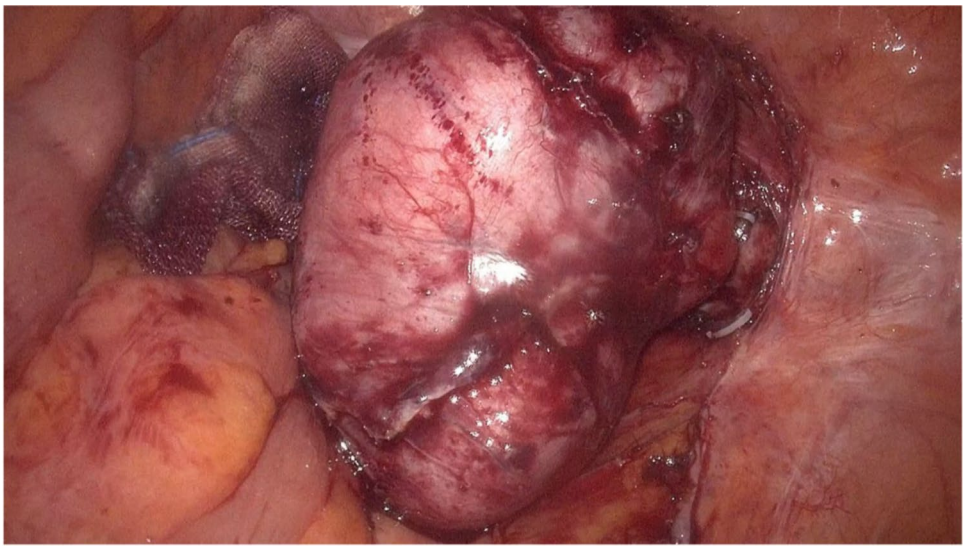

Fig. 6 The tumor was located in the retroperitoneum and exhibited lobular morphology

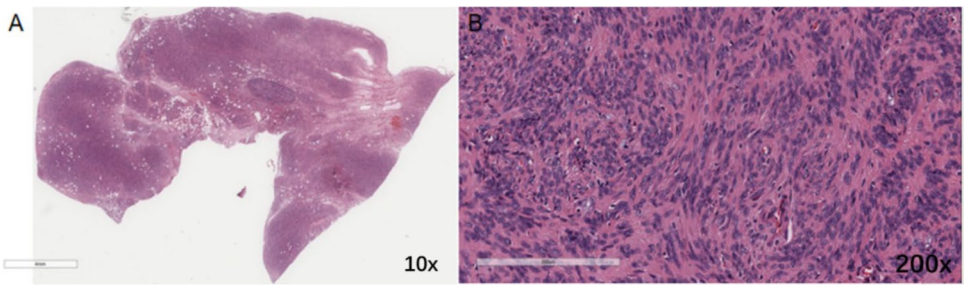

Fig. 7 The tumor in the left wall of the vaginal stump displayed well-defined boundaries, consisting of spindle cell bundles with mild cytological atypia. Features included eosinophilic cytoplasm, cigar-shaped nuclei, rare nuclear divisions, unapparent nucleoli, abundant local blood vessels, and richness in fat cells, with no necrosis or high-grade morphological features observed. (A-B correspond to H&E staining at × 10 and × 200 magnification, respectively

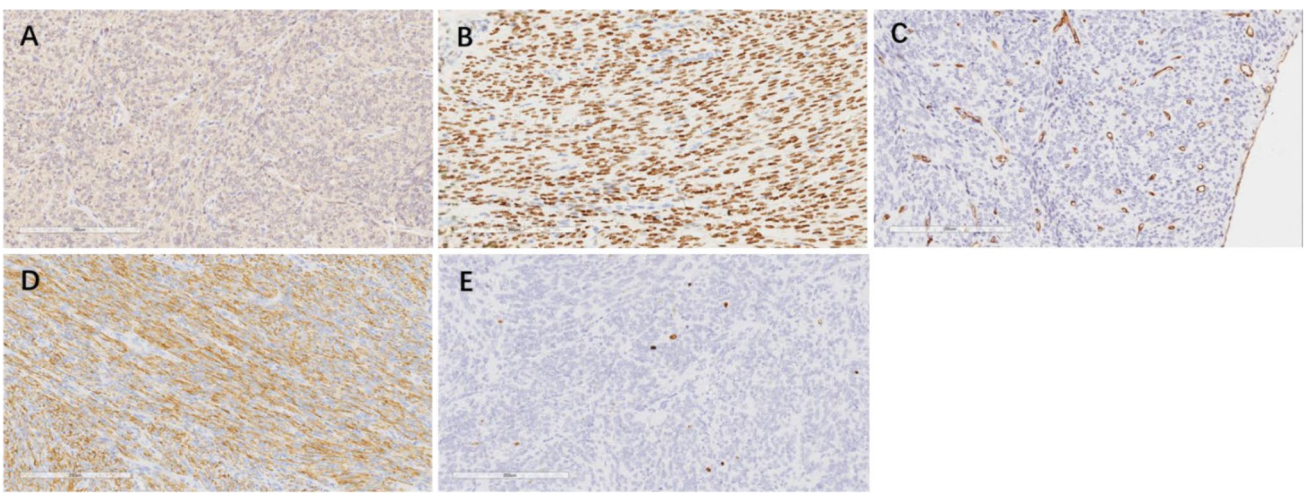

Fig. 8 **A** IHC showed positive SMA expression in the cytoplasm of spindle cells. **B** IHC indicated ER expressions in the nuclei of spindle cells. **C** IHC revealed positive CD34 expression in the single layer of squamous epithelium covering the tumor surface, **D** h-Caldesmon positivity in the cytoplasm of spindle cells, **E** nuclear Ki-67 positivity in approximately 3% of cells. EnVision, × 200

3 Materials and methods

3.1 Sample collection and processing

This study collected formalin-fixed paraffin-embedded (FFPE) tumor specimens from patients with pulmonary BML and IVL. Three distinct samples were included: tumor tissue from pulmonary BML, intravascular tumor from IVL, and vaginal stump tumor. Following deparaffinization, genomic DNA was extracted from FFPE tissues and subjected to rigorous quality control to ensure suitability for downstream sequencing.

3.2 Library preparation and WES

DNA was fragmented into 180–280 bp fragments using a Covaris ultrasonicator. Fragments underwent end-repair, 3′-adenylation (A-tailing), and Illumina adapter ligation with T4 DNA ligase. Libraries were amplified using high-fidelity polymerase and size-selected with Agencourt SPRIselect beads. Exome regions were enriched using the Agilent SureSelect Human All Exon V6 kit for hybridization capture. Captured libraries were further amplified, quantified via the Agilent 5400 system and qPCR, and sequenced on the Illumina NovaSeq platform with 150 bp paired-end (PE150) reads.

3.3 Bioinformatics analysis

Raw sequencing data underwent quality control, alignment to the reference genome (GRCh37/hg19) using BWA, and duplicate read marking with Sambamba. Variant calling for SNPs and InDels was performed using SAMtools, while copy number variations (CNVs) were detected with CoNIFER. Functional annotation of variants was conducted using ANNOVAR, integrated with databases such as RefSeq, dbSNP, COSMIC, Gene Ontology (GO), and KEGG. A multi-tool filtering strategy (SIFT, Polyphen-2, MutationTaster, CADD, etc.) was applied with stringent thresholds (e.g., CADD > 20, Polyphen-2 HDIV > 0.957/HVAR > 0.909, FATHMM < – 1.5, REVEL > 0.5) to identify high-confidence functionally relevant variants. Comparative molecular profiling was performed across samples (pulmonary BML, IVL intravascular tumor, and vaginal stump tumor).

4 Results

This study identified unique and shared missense mutations in BML and IVL cases (Table 1). In the BML case, 15 SNP mutant genes were observed: HFM1, SCN10A, HEXA, SLC7A14, TEP1, KCNJ12, KCNJ18, DNAJB12, ACOX3, ABCC2, RASA1, ALOX15B, TCIRG1, COL5A3, and MCCC2. The IVL case presented 18 SNP mutant genes: CADPS2, GPSM2, REEP4, KCNJ12, KCNJ18, DUSP15, PDE11A, TCIRG1, KLHL33, PAH, MYO18A, FBLN7, ATP7B, MYO7A, MLKL, LRP10, KRT15, and HEPH, with mutations consistently found in both samples. Shared mutations between BML and IVL cases included TCIRG1, KCNJ12, and KCNJ18. No InDel mutations met the screening criteria.

5 Discussion

Uterine leiomyoma stands as the most common tumor in premenopausal women. Although benign, it can sometimes metastasize or implant at extrauterine locations, resulting in uncommon variants like BML, IVL, and diffuse peritoneal leiomyomatosis [3]. BML typically manifests in patients with pre-existing uterine leiomyoma and is frequently linked to distant metastasis to extrauterine sites [1]. The lungs constitute the primary metastatic site, with secondary involvement of bone, spine, lymph nodes, retroperitoneum, blood vessels, skin, and the central nervous system [4, 5]. The age at diagnosis of BML is between 22 and 77 years, averaging 47.3 years [6]. IVL, marked by its proliferation along venous vessels, extends within veins, frequently reaching the uterine veins, internal iliac veins, common iliac veins, inferior vena cava,

Table 1 Unique and shared genes of BML and IVL after WES and further screening

Case 1 : CHROM	GeneName	AAChange	cytoBand	SIFT	Polyphen2_HDIV	Polyphen2_HVAR
1	HFM1	HFM1:NM_001017975:exon31:c.G3470A:p.C1157Y	1p22.2	0.0,D	1.0,D	0.994,D
3	SCN10A	SCN10A:NM_001293306:exon2:c.G308T:p.R103L,SCN10A:NM_001293307:exon2:c.G308T:p.R103L,SCN10A:NM_006514:exon2:c.G308T:p.R103L	3p22.2	0.0,D	1.0,D	0.997,D
3	SLC7A14	SLC7A14:NM_020949:exon6:c.G988A:p.G330R	3q26.2	0.006,D	0.998,D	0.969,D
4	ACOX3	ACOX3:NM_001375789:exon9:c.G779A:p.R260H,ACOX3:NM_001101667:exon10:c.G1064A:p.R355H,ACOX3:NM_001375783:exon10:c.G1064A:p.R355H,ACOX3:NM_001375784:exon10:c.G992A:p.R331H,ACOX3:NM_001375785:exon10:c.G1064A:p.R355H,ACOX3:NM_001375786:exon10:c.G1064A:p.R355H,ACOX3:NM_001375787:exon10:c.G1064A:p.R355H,ACOX3:NM_001375788:exon10:c.G1064A:p.R355H,ACOX3:NM_001375790:exon10:c.G1064A:p.R355H,ACOX3:NM_003501:exon10:c.G1064A:p.R355H	4p16.1	0.0,D	1.0,D	1.0,D
5	RASA1	RASA1:NM_002890:exon7:c.A1058G:p.H353R,RASA1:NM_022650:exon7:c.A527G:p.H176R	5q14.3	0.002,D	1.0,D	0.999,D
5	MCCC2	MCCC2:NM_001363147:exon13:c.T1172C:p.V391A,MCCC2:NM_022132:exon14:c.T1286C:p.V429A	5q13.2	0.0,D	0.988,D	0.955,D
10	DNAJB12	DNAJB12:NM_001002762:exon3:c.A335G:p.Y112C,DNAJB12:NM_001365080:exon3:c.A335G:p.Y112C,DNAJB12:NM_001365081:exon3:c.A335G:p.Y112C,DNAJB12:NM_017626:exon3:c.A335G:p.Y112C	10q22.1	0.0,D	1.0,D	0.997,D
10	ABCC2	ABCC2:NM_000392:exon18:c.C2366T:p.S789F	10q24.2	0.0,D	1.0,D	0.999,D
11	**TCIRG1**	**TCIRG1:NM_006053:exon14:c.T1616C:p.V539A,TCIRG1:NM_001351059:exon18:c.T1370C:p.V457A,TCIRG1:NM_006019:exon19:c.T2264C:p.V755A**	**11q13.2**	**0.001,D**	**0.997,D**	**0.963,D**
14	TEP1	TEP1:NM_001319035:exon24:c.A3482G:p.D1161G,TEP1:NM_007110:exon26:c.A3806G:p.D1269G	14q11.2	0.007,D	1.0,D	1.0,D
15	HEXA	HEXA:NM_000520:exon1:c.G200A:p.R67H,HEXA:NM_001318825:exon1:c.G200A:p.R67H	15q23	0.0,D	1.0,D	1.0,D
17	**KCNJ12,KCNJ18**	**KCNJ18:NM_001194958:exon3:c.C467T:p.P156L,KCNJ12:NM_021012:exon3:c.C467T:p.P156L**	**17p11.2**	**0.019,D**	**1.0,D**	**1.0,D**
17	ALOX15B	ALOX15B:NM_001039131:exon12:c.G1789C:p.E597Q,ALOX15B:NM_001039130:exon13:c.G1924C:p.E642Q,ALOX15B:NM_001141:exon14:c.G2011C:p.E671Q	17p13.1	0.0,D	1.0,D	0.999,D
19	COL5A3	COL5A3:NM_015719:exon20:c.C1771T:p.P591S	19p13.2	0.045,D	0.999,D	0.922,D

Case 1 : CHROM	LRT	MutationTaster	MutationAssessor	FATHMM	CADD	REVEL	BML	IVL_1	IVL_2	-
1	0.000,D	1.000,D	2.42,M	− 4.26,D	4.577081,32	0.806	0/1:7:118,0,93:4:3,4	0/0:5:.:.:.	0/0:5:.:.:.	–
3	0.000,D	0.999,D	3.265,M	− 2.99,D	4.465034,32	0.883	0/1:115:255,0,255:0:66,49	0/0:50:.:.:.	0/0:50:.:.:.	–
3	0.000,D	1,D	3.44,M	− 4.03,D	4.419735,32	0.762	0/1:155:255,0,255:1:82,73	0/0:50:.:.:.	0/0:50:.:.:.	–
4	0.000,D	1,D	4.175,H	− 1.89,D	3.832708,26.5	0.872	0/1:162:255,0,255:3:100,62	0/0:100:.:.:.	0/0:100:.:.:.	–
5	0.000,D	1,D	3.33,M	− 4.53,D	3.681611,25.7	0.956	0/1:16:119,0,255:22:10,6	0/0:10:.:.:.	0/0:10:.:.:.	–
5	0.000,D	1,D	4.08,H	− 2.08,D	3.342569,24.5	0.840	0/1:164:255,0,255:3:87,77	0/0:70:.:.:.	0/0:100:.:.:.	–
10	0.000,D	1,D	4.45,H	− 3.17,D	4.101255,28.6	0.929	0/1:33:255,0,255:0:18,15	0/0:50:.:.:.	0/0:30:.:.:.	–
10	0.000,D	1,D	3.665,H	**− 2.13,D**	3.708884,25.8	0.720	0/1:39:255,0,255:3:22,17	0/0:30:.:.:.	0/0:50:.:.:.	–
11	**0.000,D**	**1,D**	**2.83,M**	− 2.43,D	**3.452082,24.8**	**0.867**	**0/1:10:55,0,206:0:8,2**	**0/0:11:.:.:.**	**0/0:10:.:.:.**	–

Table 1 (continued)

Case 1 : CHROM	LRT	MutationTaster	MutationAssessor	FATHMM	CADD	REVEL	BML	IVL_1	IVL_2	-
14	0.000,D	1.000,D	2.945,M	− 2.79,D	4.241615,29.8	0.901	0/1:110:255,0,255:1:58,52	0/0:100:.:.:.	0/0:101:.:.:.	–
15	0.000,D	1.000,D	3.505,H	**− 3.43,D**	4.447559,32	0.777	0/1:213:255,0,255:1:110,102	0/0:100:.:.:.	0/0:101:.:.:.	–
17	**0.000,D**	**1,D**	**2.985,M**	− 2.66,D	**4.119805,28.8**	**0.787**	**0/1:255,0,255:118:15:77,41**	**0/1:255,0,255:210:5:108,102**	**0/1:255,0,255:220:7:119,100**	–
17	0.000,D	0.989,D	3.425,M	− 3.2,D	3.508932,25.0	0.616	0/1:50:255,0,255:4:28,22	0/0:75:.:.:.	0/0:100:.:.:.	–
19	0.000,D	1.000,D	1.95,M	FATHMM	3.361334,24.5	0.604	0/1:44:255,0,255:4:24,20	0/0:50:.:.:.	0/0:50:.:.:.	–

Case 2 : CHROM	GeneName	AAChange	cytoBand	SIFT	Polyphen2_HDIV	Polyphen2_HVAR
1	GPSM2	GPSM2:NM_001321038:exon11:c.C1216T:p.R406W,GPSM2:NM_001321039:exon11:c.C1216T:p.R406W,GPSM2:NM_013296:exon11:c.C1216T:p.R406W	1p13.3	0.0,D	1.0,D	0.995,D
2	PDE11A	PDE11A:NM_001077196:exon12:c.T935A:p.L312Q,PDE11A:NM_001077358:exon14:c.T1193A:p.L398Q,PDE11A:NM_016953:exon15:c.T2267A:p.L756Q,PDE11A:NM_001077197:exon16:c.T1517A:p.L506Q	2q31.2	0.001,D	1.0,D	0.992,D
2	FBLN7	FBLN7:NM_001128165:exon2:c.G167A:p.R56H,FBLN7:NM_153214:exon2:c.G167A:p.R56H	2q13	0.0,D	1.0,D	0.999,D
7	CADPS2	CADPS2:NM_001009571:exon1:c.C325T:p.R109W,CADPS2:NM_001167940:exon1:c.C325T:p.R109W,CADPS2:NM_001363389:exon1:c.C325T:p.R109W,CADPS2:NM_001363390:exon1:c.C325T:p.R109W,CADPS2:NM_001363391:exon1:c.C325T:p.R109W,CADPS2:NM_001363392:exon1:c.C325T:p.R109W,CADPS2:NM_001363393:exon1:c.C325T:p.R109W,CADPS2:NM_001363394:exon1:c.C325T:p.R109W,CADPS2:NM_001363395:exon1:c.C325T:p.R109W,CADPS2:NM_001363396:exon1:c.C325T:p.R109W,CADPS2:NM_001363397:exon1:c.C325T:p.R109W,CADPS2:NM_001363398:exon1:c.C325T:p.R109W,CADPS2:NM_017954:exon1:c.C325T:p.R109W	7q31.32	0.0,D	1.0,D	0.998,D
8	REEP4	REEP4:NM_001316964:exon4:c.A200C:p.E67A,REEP4:NM_001316965:exon4:c.A200C:p.E67A,REEP4:NM_025232:exon4:c.A200C:p.E67A	8p21.3	0.001,D	0.999,D	0.995,D
11	**TCIRG1**	**TCIRG1:NM_006053:exon10:c.G1096A:p.G366S,TCIRG1:NM_001351059:exon14:c.G850A:p.G284S,TCIRG1:NM_006019:exon15:c.G1744A:p.G582S**	**11q13.2**	**0.031,D**	**1.0,D**	**1.0,D**
11	MYO7A	MYO7A:NM_000260:exon28:c.C3610G:p.P1204A,MYO7A:NM_001127180:exon28:c.C3610G:p.P1204A,MYO7A:NM_001369365:exon29:c.C3577G:p.P1193A	11q13.5	0.0,D	1.0,D	1.0,D
12	PAH	PAH:NM_000277:exon7:c.C721T:p.R241C,PAH:NM_001354304:exon8:c.C721T:p.R241C	12q23.2	0.043,D	1.0,D	0.993,D
13	ATP7B	ATP7B:NM_001005918:exon9:c.C2354T:p.P785L,ATP7B:NM_001330579:exon11:c.C2723T:p.P908L,ATP7B:NM_001330578:exon12:c.C2741T:p.P914L,ATP7B:NM_000053:exon13:c.C2975T:p.P992L,ATP7B:NM_001243182:exon14:c.C2642T:p.P881L	13q14.3	0.001,D	1.0,D	1.0,D
14	KLHL33	KLHL33:NM_001109997:exon2:c.G832A:p.G278R,KLHL33:NM_001365790:exon3:c.G1624A:p.G542R	14q11.2	0.0,D	1.0,D	0.999,D

Table 1 (continued)

Case 2 : CHROM	GeneName	AAChange	cytoBand	SIFT	Polyphen2_HDIV	Polyphen2_HVAR
14	LRP10	LRP10:NM_001329226:exon7:c.G1652A:p.R551H,LRP10:NM_014045:exon7:c.G1652A:p.R551H	14q11.2	0.011,D	1.0,D	0.994,D
16	MLKL	MLKL:NM_152649:exon6:c.G865A:p.G289R	16q23.1	0.0,D	1.0,D	0.975,D
17	**KCNJ12,KCNJ18**	**KCNJ18:NM_001194958:exon3:c.C467T:p.P156L,KCNJ12:NM_021012:exon3:c.C467T:p.P156L**	**17p11.2**	**0.019,D**	**1.0,D**	**1.0,D**
17	MYO18A	MYO18A:NM_001346767:exon17:c.C2804T:p.T935I,MYO18A:NM_001346768:exon17:c.C1430T:p.T477I,MYO18A:NM_078471:exon17:c.C2804T:p.T935I,MYO18A:NM_203318:exon17:c.C2804T:p.T935I,MYO18A:NM_001346766:exon18:c.C2840T:p.T947I,MYO18A:NM_001346765:exon19:c.C2861T:p.T954I	17q11.2	0.024,D	1.0,D	0.994,D
17	KRT15	KRT15:NM_002275:exon2:c.G550C:p.A184P	17q21.2	0.001,D	0.998,D	0.985,D
20	DUSP15	DUSP15:NM_001012644:exon6:c.G64C:p.A22P,DUSP15:NM_001320478:exon6:c.G364C:p.A122P,DUSP15:NM_001320479:exon6:c.G364C:p.A122P,DUSP15:NM_080611:exon6:c.G373C:p.A125P,DUSP15:NM_177991:exon6:c.G64C:p.A22P	20q11.21	0.016,D	1.0,D	0.998,D
X	HEPH	HEPH:NM_001130860:exon4:c.G484T:p.G162C,HEPH:NM_001282141:exon4:c.G484T:p.G162C,HEPH:NM_001367232:exon4:c.G484T:p.G162C,HEPH:NM_001367233:exon4:c.G484T:p.G162C,HEPH:NM_001367234:exon4:c.G484T:p.G162C,HEPH:NM_001367236:exon4:c.G484T:p.G162C,HEPH:NM_001367238:exon4:c.G484T:p.G162C,HEPH:NM_001367239:exon4:c.G484T:p.G162C,HEPH:NM_001367240:exon4:c.G484T:p.G162C,HEPH:NM_001367241:exon4:c.G484T:p.G162C,HEPH:NM_001367243:exon4:c.G484T:p.G162C,HEPH:NM_138737:exon4:c.G637T:p.G213C	Xq12	0.014,D	0.996,D	0.924,D

Case 2 : CHROM	LRT	MutationTaster	Mutation-Assessor	FATHMM	CADD	REVEL	BML	IVL_1	IVL_2	–
1	0.000,D	1,D	2.425,M	– 3.61,D	4.251547,29.9	0.828	0/0:.:30:.:.	0/1:230,0,242:20:2:10,10	0/1:125,0,255:20:0:14,6	–
2	0.000,D	1,D	3.19,M	– 2.2,D	4.104746,28.6	0.933	0/0:.:100:.:.	0/1:255,0,255:50:3:19,31	0/1:255,0,255:65:5:27,38	–
2	0.000,D	1.000,D	2.36,M	– 1.76,D	3.942056,27.2	0.560	0/0:.:30:.:.	0/1:255,0,255:72:0:35,37	0/1:255,0,255:78:0:44,32	–
7	0.000,D	1.000,D	2.6,M	– 2.01,D	4.529758,32	0.674	0/0:.:50:.:.	0/1:255,0,255:94:3:59,35	0/1:255,0,255:108:2:57,51	–
8	0.000,D	0.999,D	2.765,M	– 3.08,D	4.141454,29.0	0.809	0/0:.:100:.:.	0/1:255,0,255:125:4:59,66	0/1:255,0,255:197:0:106,91	–
11	**0.000,D**	**1,D**	**3.67,H**	**– 3.35,D**	**4.090425,28.5**	**0.947**	**0/0:.:50:.:.**	**0/1:255,0,255:102:2:50,52**	**0/1:255,0,255:118:3:77,41**	–
11	0.000,D	1,D	3.805,H	– 3.82,D	3.862422,26.6	0.943	0/0:.:50:.:.	0/1:255,0,255:62:4:30,32	0/1:255,0,255:101:8:52,49	–
12	0.000,D	1,D	2.23,M	– 6.17,D	4.046592,28.1	0.857	0/0:.:100:.:.	0/1:255,0,255:130:3:67,63	0/1:255,0,255:136:4:71,65	–
13	0.000,D	1,D	4.44,H	– 2.37,D	3.913703,27.0	0.905	0/0:.:50:.:.	0/1:255,0,255:88:2:40,48	0/1:255,0,255:131:4:74,57	–
14	0.000,D	1.000,D	3.08,M	– 2.08,D	4.067060,28.3	0.897	0/0:.:100:.:.	0/1:255,0,255:193:1:103,90	0/1:255,0,255:214:0:124,90	–
14	0.000,D	1.000,D	2.3,M	– 3.43,D	3.619073,25.4	0.555	0/0:.:38:.:.	0/1:255,0,255:64:2:38,26	0/1:255,0,255:87:4:47,40	–
16	0.000,D	0.998,D	2.98,M	– 2.59,D	3.762598,26.1	0.726	0/0:.:100:.:.	0/1:255,0,255:77:0:43,34	0/1:255,0,255:98:3:48,50	–
17	**0.000,D**	**1,D**	**2.985,M**	**– 3.43,D**	**4.119805,28.8**	**0.787**	**0/1:255,0,255:118:15:77,41**	**0/1:255,0,255:210:5:108,102**	**0/1:255,0,255:220:7:119,100**	–
17	0.000,D	1.000,D	2.755,M	– 2.29,D	3.974180,27.5	0.826	0/0:.:101:.:.	0/1:255,0,255:191:1:118,73	0/1:255,0,255:203:4:113,90	–

Table 1 (continued)

Case 2 : CHROM	LRT	MutationTaster	Mutation-Assessor	FATHMM	CADD	REVEL	BML	IVL_1	IVL_2	–
17	0.000,D	1.000,D	4.275,H	– 2.58,D	3.380632,24.6	0.728	0/0:.:50:.:.	0/1:255,0,255:124:1:60,64	0/1:255,0,255:133:1:60,73	–
20	0.000,D	0.999,D	3.935,H	– 2.0,D	4.113424,28.7	0.618	0/0:.:30:.:.	0/1:255,0,255:42:0:21,21	0/1:255,0,255:42:1:21,21	–
X	0.000,D	0.864,D	3.155,M	– 5.02,D	2.755487,23.0	0.772	0/0:.:101:.:.	0/1:255,0,255:89:16:36,53	0/1:255,0,255:99:1:59,40	–

CHROM variations in chromosomesGeneName: Gene name annotation, listing the gene in which the variant is locatedAAChange: according to the transcript of amino acid change in annotations, use ", "space between each transcript, with a" : "different transcription in turn divided into the corresponding fields: name, a mutation in the gene mutation in the transcription of this ID, mutation in exon and the variation in the way of the change in cDNA (such as: C. C2768t indicates that the mutation caused a C to T mutation at position 2768 of cDNA), and the protein sequence change caused by the mutation (e.g. p.P923L indicates that the mutation caused an amino acid change from Pro to Leu at position 923 of protein sequence) CytoBand: the mutation sites of chromosome segments (by Giemas staining observation). If the variant site crosses more than one segment, it is connected by short horizontal linesSIFT: SIFT score (dbNSFP version3.0), said that the variation of the effect on the protein sequence. Respectively before and after the comma is SIFT_score and SIFT_pred: SIFT_score is SIFT score, score the smaller may be "harmful", suggests that the SNPS lead to the possibility of a change in protein structure or function. SIFT_pred is predicted results, the values for T or D. When the variation also affect multiple protein sequence of each protein sequences have a SIFT value, minimum value. D: Deleterious (sift<=0.05); T: Tolerated (sift > 0.05))Polyphen2_HDIV: using PolyPhen2 HumanDiv based database to predict the variation of the effect on the protein sequence, for complex diseases (dbNSFP version3.0). Before and after the comma are Polyphen2_HDIV_score and Polyphen2_HDIV_pred: Polyphen2_HDIV_score is the PolyPhen 2 score, the higher the value, the more likely to be "harmful", indicating that the SNP is more likely to cause changes in the structure or function of the protein. Polyphen2_HDIV_pred is the prediction result, with the value D or P or B (D: Probably damaging (>=0.957), P: Possibly damaging (0.453<=pp2_hdiv<=0.956). B: Benign (pp2_hdiv < = 0.452))Polyphen2_HVAR: PolyPhen2 was used to predict the effect of the variant on the protein sequence based on the HumanVar database for monogenic genetic diseases (dbNSFP version3.0). This column contains two values, the first is the PolyPhen 2 score, the greater the value is "bad", suggests that the SNPS lead to the possibility of a change in protein structure or function; The second is the D/P or B (D: Probably damaging (> = 0.909), P: Possibly damaging (0.447 < = pp2_hvar < = 0.909); B: Benign (pp2_hvar<=0.446))Prediction of LRT, LRT (dbNSFP version3.0), said that the variation of the effect on the protein sequence. Respectively before and after the comma is LRT_score and LRT_predLRT_score LRT score, score the smaller may be "harmful", suggests that the SNPS lead to the possibility of a change in protein structure or function. LRT_pred is predicted as a result, the value for D, N, or U (D: Deleterious; N: Neutral; U: Unknown)MutationTaster: MutationTaster prediction result (dbNSFP version3.0), indicating the effect of the mutation on the protein sequence. Respectively before and after the comma is MutationTaster_score and MutationTaster_pred: MutationTaster_score is MutationTaster score, the score, the greater the value of 0-1, said the more reliable results. MutationTaster_pred is the predicted result and takes the value A, D, N, or P. A" ("Disease_causing_automatic"); "D" ("Disease_causing"); "N" ("Polymorphism"); "P" (" Polymorphism_automatic "). Both A and D indicate that the site may be deleterious.MutationAssessor: MutationAssessor prediction results (dbNSFP version3.0), said that the variation of the effect on the protein sequence. Before and after the comma are MutationAssessor_score and MutationAssessor_pred: MutationAssessor_score is the MutationAssessor initial score. The higher the score, the more likely it is to be "harmful", indicating that the SNP is more likely to cause changes in protein structure or function. MutationAssessor_pred is H, M, L, or N (H: High; M: Medium; L: Low; N: Neutral). H and M denote functional, and L and N denote non-functionalFATHMM: FATHMM prediction results (dbNSFP version3.0), said that the variation of the effect on the protein sequence. Respectively before and after the comma is FATHMM_score and FATHMM_pred: FATHMM_score FATHMM initial score, score is less than 1.5 considered Deleterious, score as potentially harmful, shows that the SNPS lead to the possibility of a change in protein structure or function. FATHMM_pred is D or T (D: Deleterious; T: Tolerated)CADD: CADD is a tool for scoring the harmfulness of SNVS and indels. The integration of a variety of information to comment the function of the mutation sites; Not only predictive coding area variation (including synonymous mutations and non-synonymous mutations) function influence, also predicted variation function of non-coding regions. Our comments results, score, respectively before and after the comma is CADD and CADD_Phred; CADD column is the initial score, score CADD_Phred is transformed; CADD_Phred score, Beijing's grain to source technology co., LTD. Web site: www.novogene.com email: service@novogene.com tel: , 010-8283, 780110, said score ranking in the top 10%, 20, said the top 1%, 30, said the top 0.1%. For indels, scores are given for all indels with CADD scores, and ". means no CADD scores. For SNPS, only SNPS ranked in the top 10% of CADD scores are given, with ". indicating that the CADD score is not ranked in the top 10%. CADD author suggested SNP hazardous threshold for CADD_Phred score > 15, the article showed 10 or 15; There is no suggested value for InDelREVEL is a method that integrates multiple software prediction scores to predict the pathogenicity of rare missense mutations. The range of REVEL score was 0-1, and the higher the score was, the more harmful it was. In the literature, when the authors set a score of 0.5, the sensitivity and specificity of detecting harmful mutations were 0.754 and 0.891BML representative cases of a specimen, IVL_1, IVL_2 represent 2 cases pelvic cavity, blood vessels in the mass of sample. Use ":" divide the several fields: the site Genotype (Genotype) (homozygous: 0/0, 1/1; Hybrid: 0/1); Standardized genotype likelihood (comma-separated values corresponding to 0/0, 0/1, and 1/1 genotypes, the smaller the better); The sequencing of the depth of the total number of reads (cover); The number of reads covering the REF and ALT bases (two values separated by commas)

Discover Oncology (2025) 16:939 | https://doi.org/10.1007/s12672-025-02551-x

Table 2 Differential Diagnosis of BML: Morphological and Immunohistochemical Differences

Disease	Morphological Features	Immunohistochemistry
BML [39, 40]	Bland spindle cells without significant atypia, mitotic figures ≤ 5/10 HPF, no tumor necrosis	Desmin/SMA/h-Caldesmon (+), ER/PR (3 +), Ki-67 < 5%
MLMS [41, 42]	Marked nuclear atypia, frequent mitotic figures (≥ 10/10 HPF), often accompanied by coagulative tumor necrosis	Desmin/SMA/h-Caldesmon (+), ER/PR (- or 1 +), Ki-67 > 10%
PPL [43]	Morphologically similar to BML but with no history of uterine leiomyoma	Desmin/SMA/h-Caldesmon (+), ER/PR (- or 1 +), Ki-67 < 5%
PLAM [44]	Predominantly cystic lesions with nodular distributions of spindle cells around the cystic walls	Desmin/SMA/h-Caldesmon (+), ER/PR (- or 1 +), HMB45/Melan-A (+)
PSFT [45]	Alternating hypercellular and hypocellular areas with "staghorn" vasculature and dense collagen deposition	CD34/STAT6 (+), Desmin/SMA/h-Caldesmon (-)
PFLH [46, 47]	Cleft-like epithelium visible within the tumor, thick-walled vascular smooth muscle at the tumor periphery adjacent to or merging with the tumor	Desmin/SMA/h-Caldesmon (+), ER/PR (-), Ki-67 < 5%

The abbreviations for disease names in the table correspond to the following full terms: Metastatic Leiomyosarcoma is abbreviated as MLMS; Primary Pulmonary Leiomyoma is abbreviated as PPL; Pulmonary Lymphangioleiomyomatosis is abbreviated as PLAM; Pulmonary Solitary Fibrous Tumor is abbreviated as PSFT; Pulmonary Fibroleiomyomatous Hamartoma is abbreviated as PFLH. The forward slash "/" denotes the meaning of " and "

Discover Oncology (2025) 16:939 | https://doi.org/10.1007/s12672-025-02551-x

Table 3 Differential Diagnosis of IVL: Morphological and Immunohistochemical Differences

Disease	Morphological Features	Immunohistochemistry
IVL [48, 49]	Tumor growth within blood vessels, appearing cord-like, with no malignant features, covered by vascular endothelial cells	SMA/Desmin/h-Caldesmon (+), ER/PR (3+), Ki-67 < 5%
UL [41]	Well-differentiated bland spindle cells in fascicular arrangement. Mitotic figures < 5/10 HPF, no tumor necrosis	SMA/Desmin/h-Caldesmon (+), ER/PR (3+), Ki-67 < 5%
ULMS [41]	Marked nuclear atypia, frequent mitotic figures (≥ 10/10 HPF), and coagulative tumor necrosis	SMA/Desmin/h-Caldesmon (+), ER/PR (- or 1+), Ki-67 > 10%
LG-ESS [50]	Uniform, densely packed ovoid or spindle cells with 'tongue-like' infiltrative growth and small arteriole-like vessels; low mitotic activity	CD10 (+), ER/PR (3+). SMA/Desmin/h-Caldesmon (-)

The abbreviations for disease names in the table correspond to the following full terms: Uterine Leiomyoma is abbreviated as UL; Uterine Leiomyosarcoma is abbreviated as ULMS; Low-Grade Endometrial Stromal Sarcoma is abbreviated as LG-ESS

and occasionally the right atrium and pulmonary artery, following venous return pathways, typically without venous wall invasion [7]. In some cases, it progresses to the inferior vena cava via the ovarian vein.

5.1 Clinical manifestations

Pulmonary BML exhibits a slow progression, with most patients remaining asymptomatic, often incidentally identified during routine physical examinations. Symptoms, if present, may include shortness of breath, cough, and recurrent respiratory infections, though chest pain is rare [3]. IVL's clinical presentation varies with the extent of involvement. In its initial stage, confined to the uterus, symptoms mimic those of uterine leiomyoma [8]. However, when the disease extends to extrapelvic veins, particularly the inferior vena cava, it may induce congestive heart failure syndrome, accompanied by abnormal venous return, chest pain, peripheral edema, syncope, and pulmonary embolism [3].

5.2 Imaging studies

Chest CT of pulmonary BML typically manifests as multiple scattered solid nodules in both lungs, varying from a few millimeters to several centimeters in diameter, with well-defined boundaries, smooth edges, and homogeneous central density, devoid of lobulation [9]. In some cases, a single solitary nodule may be present in one lung. Imaging techniques offer limited diagnostic utility for IVL. When involving extrauterine blood vessels, IVL may appear as widening of the iliac vein and inferior vena cava, characterized by smooth walls and relatively free, worm-like or string-beaded masses [10]. Detection of beaded, strip-like, worm-like, or solid masses with abundant blood supply in the pelvic blood vessels through imaging or surgery should prompt suspicion of IVL, which must be confirmed via pathological examination.

5.3 Pathology

BML, IVL, and conventional uterine leiomyoma share nearly identical histological features. All three entities present as well-circumscribed solid masses composed of intersecting fascicles of spindle-shaped smooth muscle cells demonstrating uniform cellularity, well-differentiated morphology with evenly distributed chromatin, typically exhibiting < 5 mitoses/10 HPF, and lacking significant nuclear atypia or tumor necrosis—features that collectively exclude malignancy. Immunohistochemically, they consistently express desmin, SMA, h-caldesmon, ER, and PR [11]. However, their biological behaviors diverge markedly. Uterine leiomyoma demonstrates purely localized uterine growth without invasive or metastatic potential. In contrast, BML, while histologically indistinguishable from primary uterine leiomyoma, exhibits distant metastases (particularly to lungs and lymph nodes) where tumor deposits grow as multiple well-demarcated nodules [2, 12]. IVL characteristically shows intravascular worm-like or cord-like tumor projections lined by CD31/CD34-positive endothelial cells, frequently accompanied by myxoid or hyaline degeneration but maintaining benign cytological features. The tumor cells of IVL exhibit worm-like or cord-like growth patterns along venous channels, with the tumor surface characteristically lined by CD31/CD34-positive vascular endothelial cells. These lesions frequently demonstrate myxoid or hyaline degeneration but maintain benign cytological features and lack distant metastatic potential [13]. Additional differential diagnostic features between BML and IVL are summarized in Tables 2 and 3.

5.4 Treatments

Currently, no standard treatment regimen exists for BML. Treatment strategies vary based on clinical manifestations and symptom severity. Effective options reported include observation, surgical resection, hysterectomy, bilateral oophorectomy, progestin, aromatase inhibitors, and luteinizing hormone-releasing hormone analogs for medical castration [14, 15]. Asymptomatic or stable patients may be managed with observation. Surgical intervention is typically preferred for larger solitary tumors [3]. Endocrine therapy may be considered for multiple tumors that are not amenable to complete resection [16]. Radical surgery remains the most effective treatment for IVL, with no recurrence reported following complete resection of circulatory system tumors combined with total hysterectomy and bilateral adnexectomy [17].

BML and IVL in this report corresponded with documented clinical manifestations, imaging results, intraoperative findings, and pathological outcomes. Treatment predominantly involved surgical tumor excision and endocrine therapy. BML typically manifests as rare, unexplained chest pain. In the IVL case, tumor growth extended into the vaginal stump, in addition to venous involvement. However, multiple pulmonary nodules observed in the IVL case were not pathologically confirmed as IVL dissemination.

Discover Oncology (2025) 16:939 | https://doi.org/10.1007/s12672-025-02551-x

Table 4 Previous Molecular Studies on BML and IVL

Authors	Disease	Case Number	Sample Type	Detection Method	Key Findings
Nucci et al. [20]	BML	5 cases	Fresh tissue	-	High-frequency deletions in 19q and 22q suggest BML may originate from a distinct subgroup of uterine leiomyomas
Bowen et al. [51]	BML	1 case	FFPE	FISH	HMGA1 (6p21) gene rearrangements in most BMLs, indicating homology between BML and uterine leiomyoma
Sõritsa et al. [21]	BML	1 case	FFPE	WES	BMP8B (c.1139A > G) mutation may promote BML metastasis
Jiang et al. [22]	BML	1 case	FFPE	WES	PTEN (c.492 + 1G > A) mutation may serve as a biomarker for PBML biology
Dal Cin et al. [52]	IVL	2 cases	-	Karyotyping, FISH	Extra copies of 12q15-qter and/or deletions of 14q24-qter may be key to IVL vascular invasion
Ordulu et al. [26]	IVL	12 cases	FFPE	FISH	Significant association between MGA2 expression and t(12;14)(q15;q24), which may drive IVL pathogenesis
Hu et al. [49]	IVL	17 cases	FFPE	Sanger sequencing	MED12 mutations may activate pathways in IVL distinct from conventional leiomyomas
Ordulu et al. [48]	IVL	28 cases	FFPE	aCGH	Molecular subgroups identified: del(22q) group and del(10q) group; del(10q) and del(22q) are mutually exclusive
Our study	BML,IVL	1 case each	FFPE	WES	Mutations in TCIRG1, KCNJ12, and KCNJ18 genes may correlate with tumor aggressiveness in both diseases

The abbreviations in the table correspond to the following full terms: Formalin-Fixed Paraffin-Embedded Tissue is abbreviated as FFPE; Fluorescence In Situ Hybridization is abbreviated as FISH; array-based Comparative Genomic Hybridization is abbreviated as aCGH. The forward slash "/" denotes the meaning of " and "

Table 5 Shared Mutation Types in BML and IVL

Sample Name	GeneName	Func	ExonicFunc	AAChange	cytoBand
S1, S2, S3	KCNJ12	exonic	missense SNV	NM_021012:exon3:c.C467T:p.P156L	17p11.2
S1, S2, S3	KCNJ18	exonic	missense SNV	NM_001194958:exon3:c.C467T:p.P156L	17p11.2
S1	TCIRG1	exonic	missense SNV	NM_006053:exon14:c.T1616C:p.V539A, NM_001351059:exon18:c.T1370C:p.V457A, NM_006019:exon19:c.T2264C:p.V755A	11q13.2
S2, S3	TCIRG1	exonic	missense SNV	NM_006053:exon10:c.G1096A:p.G366S, NM_001351059:exon14:c.G850A:p.G284S, NM_006019:exon15:c.G1744A:p.G582S	11q13.2

S1 is the name of the pulmonary tumor sample from a BML patient, while S2 and S3 represent the intravascular tumor sample and the vaginal stump tumor sample names from IVL patients, respectively

5.5 Genetics and spread mechanism

The pathogenesis of BML remains uncertain, with prevailing hypotheses encompassing lymphatic and vascular dissemination of uterine leiomyoma, peritoneal seeding, and coelomic metaplasia [18]. The predominant theory posits that tumor cells enter the bloodstream during uterine surgery and subsequently disseminate via blood vessels [19]. Genetic alterations linked to BML have been documented in various studies (Table 4). Nucci et al. [20] found genetic similarities between BML and uterine leiomyoma, such as deletions on chromosomes 19q and 22q deletions, suggesting a common origin. A study demonstrated heterozygous mutations in the BMP8B gene (c.1139A > G, Tyr380Cys) specifically in pulmonary BML but not in blood or uterine leiomyoma, indicating a potential role in BML metastasis [21]. Despite immunohistochemical staining revealing ER and PR expression, a patient with confirmed BML experienced progressive metastatic lesions following tamoxifen treatment. WES revealed simultaneous missense mutations in BLMH, LRP2, MED12, SMAD2, and UGT1A8 in both primary uterine leiomyoma and pulmonary BML, along with a PTEN mutation (c.492 + 1G > A) in the pulmonary BML tumor [22]. PTEN, a tumor suppressor [23], when underexpressed, can activate the PI3K pathway, leading to endocrine resistance in ER-positive breast cancer [24]. The PTEN mutation likely contributes to BML metastasis and resistance to endocrine therapy.

The pathogenesis of IVL remains uncertain, with the leading hypothesis proposing hematogenous dissemination of uterine leiomyoma. Tumor extension typically follows venous return through two primary pathways [3]: one involving the uterine, internal iliac, common iliac veins, and inferior vena cava; the other involving the ovarian and renal veins, and inferior vena cava. This progression can eventually reach the right atrium and potentially extend to the pulmonary artery. Molecular studies on IVL are currently limited (Table 4). One study revealed common chromosomal abnormalities in IVL, including deletions in the 22q11.23-q13.31 and 22q12.3-q13.1 regions [25]. FISH analysis consistently detects 12q14.3 rearrangements and HMGA2 overexpression, with karyotype analysis revealing chromosome 22 deletions in two out of three cases [26]. Additional research reports upregulation of GATA2, LIF, CXCL8, SH2D2A, and ADAM8 in IVL tumors, which enhances angiogenesis and tumor dissemination [27]. Beyond its role as a pro-angiogenic factor, ADAM8 also promotes tumor spread and metastasis in breast cancer [28]. This study identified ADAM8 missense mutations in all three paraffin-embedded samples, while no HMGA2 missense mutations were detected. These data suggest a significant role for ADAM8 in the development and progression of IVL and BML.

WES analysis found 15 SNP genes in the BML case meeting further screening criteria: HFM1, SCN10A, HEXA, SLC7A14, TEP1, KCNJ12, KCNJ18, DNAJB12, ACOX3, ABCC2, RASA1, ALOX15B, TCIRG1, COL5A3, and MCCC2. In the IVL case, 18 mutant genes were observed: CADPS2, GPSM2, REEP4, KCNJ12, KCNJ18, DUSP15, PDE11A, TCIRG1, KLHL33, PAH, MYO18A, FBLN7, ATP7B, MYO7A, MLKL, LRP10, KRT15, and HEPH. Consistent mutations across both samples provide strong evidence of source consistency. The distinct deleterious mutant genes in the two cases may offer new insights into the molecular mechanisms distinguishing BML from IVL. Additionally, TCIRG1, KCNJ12, and KCNJ18 (Table 5) were identified as shared mutant genes in both BML and IVL cases.

TCIRG1, also known as V-ATPase-a3, plays a critical role in cell metabolism, membrane transport, and intracellular signal transduction through acidification. Elevated TCIRG1 expression is associated with increased invasion and metastasis in various tumors. For instance, In highly metastatic B16-F10 melanoma cells, the high expression and plasma membrane localization of TCIRG1 are closely associated with metastatic potential. TCIRG1 creates an acidic microenvironment

through its proton pump activity, which activates matrix metalloproteinases (e.g., MMP-2 and MMP-9) to degrade the extracellular matrix (ECM), thereby enhancing cellular invasiveness and migratory capacity. In contrast, TCIRG1 knockdown or treatment with specific inhibitors (e.g., FR167356) significantly suppresses invasion, migration, and distant metastasis without affecting primary tumor growth, indicating that TCIRG1 primarily functions during the metastatic stage [29]. Similarly, In invasive breast cancer cells, TCIRG1 is highly expressed on the plasma membrane and promotes microenvironment acidification by secreting protons. This process activates MMP-2/MMP-9 to accelerate extracellular matrix (ECM) degradation, thereby enhancing cellular invasion and migration. Genetic knockdown of TCIRG1 suppresses these aggressive phenotypes, whereas overexpression amplifies metastatic potential [30]. In hepatocellular carcinoma, TCIRG1 impedes tumor cell growth and proliferation, induces cell death, and promotes migration via epithelial-mesenchymal transition (EMT) [31]. In the mesenchymal subtype of glioblastoma multiforme (GBM), TCIRG1 is highly expressed and acidifies the tumor microenvironment through V-ATPase activity. This activates factors such as cathepsins and VEGF, promoting extracellular matrix (ECM) degradation and tumor angiogenesis, thereby enhancing invasive and migratory capabilities [32]. Elevated TCIRG1 expression is correlated with malignant progression and poor prognosis in ccRCC patients [33] and shows a positive association with immunosuppressants PDCD1 and CTLA4 [34].

KCNJ12 and KCNJ18 are potassium channel-related genes. Kir2.2, encoded by KCNJ12, is an inwardly rectifying potassium channel protein belonging to the potassium channel family. In prostate, gastric, and breast cancers, gain-of-function mutations in KCNJ12 may accelerate tumor progression or metastasis in p53/p16-deficient breast cancer by suppressing p27 expression through ROS reduction (thereby releasing cell cycle arrest) and maintaining mitochondrial homeostasis to sustain high-energy metabolism, ultimately bypassing senescence pathways [35]. In multiple cancers, gain-of-function mutations in *KCNJ12* drive tumor proliferation, angiogenesis, and metastasis by binding to NF-κB p65/RelA to promote its phosphorylation and nuclear translocation, thereby upregulating the expression of cyclin D1, MMP9, and VEGF. Concurrently, these mutations stabilize mitochondrial function to sustain high-energy metabolism [36]. In esophageal squamous cell carcinoma (ESCC), mutations in *KCNJ12* may influence disease progression by altering the function of the potassium channel protein Kir2.2. Studies have shown that its dysfunction can regulate cancer cell behavior through the RelA signaling pathway—for example, enhanced Ser536 phosphorylation of RelA induced by Kir2.2 overexpression promotes cancer cell proliferation [37]. Overexpression of KCNJ12 promotes bladder cancer cell proliferation, migration, invasion, differentiation, and xenograft tumor formation in vivo by activating the GSK3β/AKT signaling pathway and inducing the epithelial-mesenchymal transition (EMT) process, characterized by upregulation of N-Cadherin, Vimentin, and MMP-7. Conversely, KCNJ12 knockdown partially reverses these effects and suppresses tumor metastasis-driving mechanisms [38].

Previous research has identified TCIRG1, KCNJ12, and KCNJ18 as significant in the proliferation, invasion, migration, and metastasis of various tumors [30, 31, 34, 36]. This study detected mutations in these genes in both BML and IVL cases, with multiple predictive software classifying these mutations as harmful. This indicates that these shared mutant genes may play a key role in the pathological mechanisms underlying BML and IVL, especially in extrauterine invasion, enhancing the understanding of the relationship between these diseases and potential therapeutic targets.

Although this study revealed potential pathogenic genetic variants associated with BML and IVL through WES, the small sample size limited the statistical generalizability and accuracy of the results. Additionally, while missense mutations in genes such as **TCIRG1**, **KCNJ12**, and **KCNJ18** were identified, their precise biological effects require further experimental validation. Future work should focus on expanding the sample size and conducting functional studies to better elucidate the roles of these variants in disease pathogenesis, thereby advancing therapeutic strategies. This approach will ensure more representative and reliable findings while providing a robust scientific foundation for clinical applications.

6 Conclusion

Expanding on these findings, this study identified several potential pathogenic genes in BML and IVL through whole genome sequencing and related analyses, offering valuable insights into their pathogenesis. Further investigation into the roles and mechanisms of these genes is expected to advance understanding of BML and IVL development, potentially leading to novel diagnostic, management, and preventive strategies for related conditions.

Acknowledgements The authors would like to thank all the reviewers who participated in the review and thank Bullet Edits Limited for the linguistic editing and proofreading of the manuscript.

Author contributions Writing–original draft: J L and JF Z, Writing & editing:J L, JJ W. JF Z and S L prepared all figures.All the authors have read & approved the final manuscript.

Funding This study was supported by Zunyi Science and Technology Program [grant No. ZunShiKeHe HZ Zi(2024)194 Hao], Guizhou Population Health Foundation (grant No.2024GZYXKYJJXM0029), Science and technology Support Program of Guizhou Province (Qiankehezhicheng[2022] Yiban182).

Availability of data and materials All the data regarding the findings are available within the manuscript.

Declarations

Ethics approval and consent to participate This case report was approved by the Ethics Committee of the Affiliated Hospital of Zunyi Medical University. Written informed consent was obtained from the patient and the patient's family for publication of this clinical case report.

Consent for publication Written informed consent was obtained from the patient and the patient's family for publication of this case report and any accompanying images.

Competing interests The authors declare no competing interests.

References

1. Robboy SJ, Bentley RC, Butnor K, et al. Pathology and pathophysiology of uterine smooth-muscle tumors. Environ Health Perspect. 2000;108(Suppl 5):779–84.
2. Tong T, Fan Q, Wang Y, et al. Benign metastasizing uterine leiomyoma with lymphatic and pulmonary metastases: a case report and literature review. BMC women's health. 2023;23(1):154.
3. Boavida Ferreira J, Cabrera R, Santos F, et al. Benign metastasizing leiomyomatosis to the skin and lungs, intravenous leiomyomatosis, and leiomyomatosis peritonealis disseminata: a series of five cases. Oncologist. 2022;27(1):e89–98.
4. Barnaś E, Książek M, Raś R, et al. Benign metastasizing leiomyoma: a review of current literature in respect to the time and type of previous gynecological surgery. PLoS ONE. 2017;12(4): e0175875.
5. Fan R, Feng F, Yang H, et al. Pulmonary benign metastasizing leiomyomas: a case series of 23 patients at a single facility. BMC Pulm Med. 2020;20(1):292.
6. Miller J, Shoni M, Siegert C, et al. Benign metastasizing leiomyomas to the lungs: an institutional case series and a review of the recent literature. Ann Thorac Surg. 2016;101(1):253–8.
7. Lam PM, Lo KWK, Yu MY, et al. Intravenous leiomyomatosis: two cases with different routes of tumor extension. J Vasc Surg. 2004;39(2):465–9.
8. Lin J, Song X, Liu C. Pelvic intravascular leiomyomatosis associated with benign pulmonary metastasizing leiomyoma: Clinicopathologic, clonality, and copy number variance analysis. IJGP. 2014;33(2):140–5.
9. Hu S S, Wang L L, Zhao H, et al. [Clinicopathological features and gene phenotypes of benign metastasizing leiomyoma]. Zhonghua Bing Li Xue Za Zhi = Chinese Journal of Pathology, 2020, 49(7): 704–709.
10. Gynecologic Oncology Subgroup, Chinese Obstetricians and Gynecologists Association. [Chinese expert consensus on clinical diagnosis and treatment of pelvic venous leiomyomatosis]. Zhonghua Fu Chan Ke Za Zhi, 2023, 58(4): 252–258.
11. Liegl-Atzwanger B, Heitzer E, Flicker K, et al. Exploring chromosomal abnormalities and genetic changes in uterine smooth muscle tumors. Modern Pathol. 2016;29(10):1262–77.
12. AlQudah MA, Hamouri S, Haddad HK, et al. Pulmonary benign metastasizing leiomyoma: A report of two cases. Fut Sci OA. 2022;8(8):FSO14.
13. Tang L, Lu B. Intravenous leiomyomatosis of the uterus: a clinicopathologic analysis of 13 cases with an emphasis on histogenesis. Pathol Res Pract. 2018;214(6):871–5.

14. Ofori K, Fernandes H, Cummings M, et al. Benign metastasizing leiomyoma presenting with miliary pattern and fatal outcome: case report with molecular analysis & review of the literature. Respir Med Case Rep. 2019;27: 100831.
15. Yoon G, Kim TJ, Sung CO, et al. Benign metastasizing leiomyoma with multiple lymph node metastasis: a case report. Cancer Res Treat. 2011;43(2):131–3.
16. Lewis EI, Chason RJ, DeCherney AH, et al. Novel hormone treatment of benign metastasizing leiomyoma: an analysis of five cases and literature review. Fertil Steril. 2013;99(7):2017–24.
17. Li H, Xu J, Lin Q, et al. Surgical treatment strategies for extra-pelvic intravenous leiomyomatosis. Orphanet J Rare Dis. 2020;15(1):153.
18. Awonuga AO, Shavell VI, Imudia AN, et al. Pathogenesis of benign metastasizing leiomyoma: a review. Obstet Gynecol Surv. 2010;65(3):189–95.
19. Egberts JH, Schafmayer C, Bauerschlag DO, et al. Benign abdominal and pulmonary metastasizing leiomyoma of the uterus. Arch Gynecol Obstet. 2006;274(5):319–22.
20. Nucci MR, Drapkin R, Dal Cin P, et al. Distinctive cytogenetic profile in benign metastasizing leiomyoma: Pathogenetic implications. Am J Surg Pathol. 2007;31(5):737–43.
21. Sõritsa D, Teder H, Roosipuu R, et al. Whole exome sequencing of benign pulmonary metastasizing leiomyoma reveals mutation in the BMP8B gene. BMC Med Genet. 2018;19(1):20.
22. Jiang J, He M, Hu X, et al. Deep sequencing reveals the molecular pathology characteristics between primary uterine leiomyoma and pulmonary benign metastasizing leiomyoma. Clin Transl Oncol. 2018;20(8):1080–6.
23. Abell MR, Littler ER. Benign metastasizing uterine leiomyoma. Multiple lymph nodal metastases. Cancer. 1975;36(6):2206–13.
24. Mizuno M, Nawa A, Nakanishi T, et al. Clinical benefit of endocrine therapy for benign metastasizing leiomyoma. Int J Clin Oncol. 2011;16(5):587–91.
25. Buza N, Xu F, Wu W, et al. Recurrent chromosomal aberrations in intravenous leiomyomatosis of the uterus: High-resolution array comparative genomic hybridization study. Hum Pathol. 2014;45(9):1885–92.
26. Ordulu Z, Nucci MR, Dal Cin P, et al. Intravenous leiomyomatosis: an unusual intermediate between benign and malignant uterine smooth muscle tumors. Mod Pathol. 2016;29(5):500–10.
27. Wang W, Wang Y, Chen F, et al. Intravenous leiomyomatosis is inclined to a solid entity different from uterine leiomyoma based on RNA-seq analysis with RT-qPCR validation. Cancer Med. 2020;9(13):4581–92.
28. Romagnoli M, Mineva ND, Polmear M, et al. ADAM8 expression in invasive breast cancer promotes tumor dissemination and metastasis. EMBO Mol Med. 2014;6(2):278–94.
29. Nishisho T, Hata K, Nakanishi M, et al. The a3 isoform vacuolar type H^+-ATPase promotes distant metastasis in the mouse B16 melanoma cells. MCR. 2011;9(7):845–55.
30. McGuire CM, Collins MP, Sun-Wada G, et al. Isoform-specific gene disruptions reveal a role for the V-ATPase subunit a4 isoform in the invasiveness of 4T1-12B breast cancer cells. J Biol Chem. 2019;294(29):11248–58.
31. Yang HD, Eun JW, Lee KB, et al. T-cell immune regulator 1 enhances metastasis in hepatocellular carcinoma. Exp Mol Med. 2018;50(1): e420.
32. Qi C, Lei L, Hu J, et al. T cell immune regulator 1 is a prognostic marker associated with immune infiltration in glioblastoma multiforme. Oncol Lett. 2021;21(4):252.
33. Xu C, Jia B, Yang Z, et al. Integrative analysis identifies TCIRG1 as a potential prognostic and immunotherapy-relevant biomarker associated with malignant cell migration in clear cell renal cell carcinoma. Cancers. 2022;14(19):4583.
34. Di S, Gong M, Lv J, et al. Glycolysis-related biomarker TCIRG1 participates in regulation of renal cell carcinoma progression and tumor immune microenvironment by affecting aerobic glycolysis and AKT/mTOR signaling pathway. Cancer Cell Int. 2023;23(1):186.
35. Lee I, Park C, Kang WK. Knockdown of inwardly rectifying potassium channel Kir2.2 suppresses tumorigenesis by inducing reactive oxygen species-mediated cellular senescence. Mole Cancer Ther. 2010;9(11):2951–9.
36. Lee I, Lee SJ, Kang TM, et al. Unconventional role of the inwardly rectifying potassium channel Kir2.2 as a constitutive activator of RelA in cancer. Cancer Res. 2013;73(3):1056–62.
37. Khalilipour N, Baranova A, Jebelli A, et al. Familial esophageal squamous cell carcinoma with damaging rare/germline mutations in KCNJ12/KCNJ18 and GPRIN2 genes. Cancer Genet. 2018;221:46–52.
38. Li G, Guo BY, Wang HD, et al. CircRNA hsa_circ_0014130 function as a miR-132-3p sponge for playing oncogenic roles in bladder cancer via upregulating KCNJ12 expression. Cell Biol Toxicol. 2022;38(6):1079–96.
39. Patton KT, Cheng L, Papavero V, et al. Benign metastasizing leiomyoma: clonality, telomere length and clinicopathologic analysis. Mod Pathol. 2006;19(1):130–40.
40. Nuovo GJ, Schmittgen TD. Benign metastasizing leiomyoma of the lung: clinicopathologic, immunohistochemical, and micro-RNA analyses. Diagnostic Mol Pathol. 2008;17(3):145–50.
41. Pinto A. Uterine smooth muscle tumors: an overview. Adv Anat Pathol. 2024;31(6):397–410.
42. Bell SW, Kempson RL, Hendrickson MR. Problematic uterine smooth muscle neoplasms. A clinicopathologic study of 213 cases. Am J Surg Pathol. 1994;18(6):535–58.
43. Gal AA, Brooks JS, Pietra GG. Leiomyomatous neoplasms of the lung: a clinical, histologic, and immunohistochemical study. Mod Pathol. 1989;2(3):209–16.
44. Zhang X, Travis WD. Pulmonary lymphangioleiomyomatosis. Arch Pathol Lab Med. 2010;134(12):1823–8.
45. Vogels RJC, Vlenterie M, Versleijen-Jonkers YMH, et al. Solitary fibrous tumor—clinicopathologic, immunohistochemical and molecular analysis of 28 cases. Diagn Pathol. 2014;9:224.
46. Becker RM, Viloria J, Chiu C. Multiple pulmonary leiomyomatous hamartomas in women. J Thorac Cardiovasc Surg. 1976;71(4):631–2.
47. Okudela K, Umeda S, Otara M, et al. A case of pulmonary hamartoma with distinctive histopathological features: A discussion of its differential diagnosis and histogenesis. Pathol Int. 2014;64(12):618–23.
48. Ordulu Z, Chai H, Peng G, et al. Molecular and clinicopathologic characterization of intravenous leiomyomatosis. Mod Pathol. 2020;33(9):1844–60.

49. Lu B, Liu Q, Tang L, et al. Intravenous leiomyomatosis: molecular analysis of 17 cases. Pathology. 2020;52(2):213–7.
50. Gadducci A, Multinu F, De Vitis LA, et al. Endometrial stromal tumors of the uterus: epidemiology, pathological and biological features, treatment options and clinical outcomes. Gynecol Oncol. 2023;171:95–105.
51. Bowen JM, Cates JM, Kash S, et al. Genomic imbalances in benign metastasizing leiomyoma: characterization by conventional karyotypic, fluorescence in situ hybridization, and whole genome SNP array analysis. Cancer Genet. 2012;205(5):249–54.
52. Dal Cin P, Quade BJ, Neskey DM, et al. Intravenous leiomyomatosis is characterized by a der(14)t(12;14)(q15;q24). Genes Chromosom Cancer. 2003;36(2):205–6.